Aerosol Science and Technology

ISSN: 0278-6826 (Print) 1521-7388 (Online) Journal homepage: http://www.tandfonline.com/loi/uast20

Effects of size and shape on filtration of TiO_2 nanoparticles

Yung Sung Cheng & Yue Zhou

To cite this article: Yung Sung Cheng & Yue Zhou (2017) Effects of size and shape on filtration of TiO_2 nanoparticles, Aerosol Science and Technology, 51:8, 972-980, DOI: 10.1080/02786826.2017.1321102

To link to this article: https://doi.org/10.1080/02786826.2017.1321102

Accepted author version posted online: 04 May 2017.
Published online: 09 May 2017.

Submit your article to this journal

Article views: 460

View Crossmark data

Citing articles: 2 View citing articles

Full Terms & Conditions of access and use can be found at
http://www.tandfonline.com/action/journalInformation?journalCode=uast20

AEROSOL SCIENCE AND TECHNOLOGY
2017, VOL. 51, NO. 8, 972–980
https://doi.org/10.1080/02786826.2017.1321102

Taylor & Francis
Taylor & Francis Group

Check for updates

Effects of size and shape on filtration of TiO_2 nanoparticles

Yung Sung Cheng and Yue Zhou

Lovelace Respiratory Research Institute, Albuquerque, New Mexico, USA

ABSTRACT

Titanium dioxide (TiO_2) is one of the most widely used nanoscale materials to date and could result in human exposures. The main objective of this study was to perform detailed characterization of TiO_2 agglomerate particles and how these properties influence particle penetration in a screen filter. Transmission electron microscope (TEM) photos showed compact agglomerates of nanoscale primary particles. The projected area diameter was close to the mobility diameter, where the length was about 25% larger than the mobility diameter. The mean aspect ratio of TiO_2 agglomerate was constant between 1.39 and 1.55. Using the tandem differential mobility analyzer-aerosol particles mass analyzer (DMA-APM) technique, we were able to measure aerodynamic diameter, mass, and fractal dimension. The value of fractal dimension based on mass and mobility diameter was 2.8. Penetration of classified TiO_2 particles through a screen filter was measured. Penetration increased with increasing mobility diameter and flow rate indicating that diffusion and interception were the main filtration mechanism. The measured physical dimensions, mobility diameter, and aerodynamic diameter were used in a single-fiber filtration theory for the fan model filter to predict the penetration of TiO_2 particles. The interception parameter was the key to estimate the penetration. Experimental penetration data were in best agreement with the model in which the maximum length was used to calculate the interception model. This result was consistent with the assumption that the rotation time of a non-spherical particle of small aspect ratio was much less than the transport time for the particle to pass through the filter fiber.

ARTICLE HISTORY
Received 3 January 2017
Accepted 17 April 2017

EDITOR
Jing Wang

Introduction

The global production of TiO_2 for all uses is in the millions of tons per year. It is used in the paint, pigment, and lacquer segment at nearly 57% of the market, followed by the plastics segment at 26%, and paper with another 13%. The remaining 4% is comprised of "other" segments including applications such as catalysts, cosmetics, coated fabrics, ceramics, printing inks, roofing granules, welding fluxes, and glass. Recently, more attention has been given to the use of TiO_2 as a nanomaterial. TiO_2 is one of the most widely used nanoscale materials to date; it is incorporated into consumer products such as sunscreens and toothpastes; industrial products like paints, lacquers, and papers; and photocatalytic processes such as water treatment (Robichaud et al. 2015). Consequentially, many sources of nanoscale TiO_2 could result in human exposure and entrance of this material into the environment (air, water, or soil compartments).

TiO_2 is produced and used in the workplace in varying particle size fractions including fine (or respirable) and ultrafine (or nanoparticle <100 nm). Sampling studies at plants handling bulk TiO_2 powder showed airborne particles in the size range between 10 nm and 20 μm, indicating that nanoscale TiO_2 particles could be released from bulk powder (Huang et al. 2010; Ichihara et al. 2016). The total mass concentration in one facility was 30 mg/m^3 (Ichihara et al. 2016); whereas in another facility the TiO_2 respirable mass concentrations in the range of 6 to 142 μg/m^3 were obtained (Huang et al. 2010). In two research facilities where nanoscale TiO_2 particles were produced, mass concentrations of 0.1 to 4.99 mg/ m^3 TiO_2 were measured (Lee et al. 2011). The number particle sizes ranged between 15 and 710 nm, showing bimodal distributions. Exposure assessment at seven small to large facilities that manufactured and used nanoscale metal oxides including titanium was conducted in a study (Curwin and Bertke 2011). The mass concentrations from personal samplers had geometric means of 78 and 11 μg/m^3 for the large and medium facilities, respectively. A MOUDI cascade impactor was used to determine the mass concentration size distribution. Generally, the greater mass of particles was found in the large particle sizes. In production processes, the predominant mass of particles is found in the 0.1 to

CONTACT Yung Sung Cheng ycheng@lrri.org Lovelace Respiratory Research Institute, 2425 Ridgecrest Dr. SE, Albuquerque, NM 87108, USA.
© 2017 American Association for Aerosol Research

1 μm diameter range. Transmission electron microscope (TEM) analysis also showed that the majority of particles were compact aggregates. TEM analysis of TiO_2 particles in plants that handled bulk powder and nanoscale materials showed similar compact aggregates consisting of spherical particles (Koivisto et al. 2012; Ichihara et al. 2016).

TiO_2 is a poorly soluble and low toxicity particle. The Occupational Safety and Health Administration (OSHA) permissible exposure limit for TiO_2 is 15 mg/m^3. In a chronic inhalation study of rats exposed to 250 mg/ m^3 of fine TiO_2, increased probabilities of lung tumor were observed (Lee et al. 1985). The National Institute of Occupational Safety and Health (NIOSH) recommended that TiO_2 be classified as a potential occupational carcinogen and that exposures be controlled as low as feasible in 1988. Later, a 2-year inhalation study showed a statistically significant increase in lung cancer in rats exposed to ultrafine TiO_2 at an average concentration of 10 mg/ m^3 (Heinrich et al. 1995). Two recent epidemiologic studies have not found a relationship between exposure to total or respirable TiO_2 and lung cancer (Fryzek et al. 2003; Boffetta et al. 2004). Recently, NIOSH recommended airborne exposure limits of 2.4 mg/m^3 for fine TiO_2 and 0.3 mg/m^3 for ultrafine (including engineered nanoscale) TiO_2, as TWA concentrations for up to 10 h/ day during a 40-h work week (NIOSH 2011). NIOSH also recommended controlling exposures as low as possible.

Filtration processes are commonly used in the occupational environment to reduce the airborne particle concentration and to control worker exposure. Performance evaluation of filters and respirators using nanoparticles showed diffusion and interception are the dominant deposition mechanisms for ultrafine particles (Cheng and Yeh 1980; Ichitsubo et al. 1996; Kim et al. 2007; Rengasamy et al. 2009; Chen et al. 2014, 2015; Zhou and Cheng 2016). Experimental data agreed with the filtration theory for spherical particles in fan model filters such as screen filters (Cheng et al. 1980; Kirsch and Chechuev 1985; Ichitsubo et al. 1996) and in Nuclepore filters (Chen et al. 2015). For silver nanoparticle agglomerates of varying degree of complexity depending on the temperature treatment, penetration through as a screen filter showed lower penetration than spherical particles of the same mobility diameter (Kim et al. 2009). Detailed characteristics of silver nanoparticles including mobility, diameter, mass, and maximum length were used in the filtration model to explain the experimental data. Chen et al. (2015) further demonstrated that penetrations of silver aggregates in a Nuclepore filter decreased as the mass–mobility fractal dimension decreased from 3.0 to 2.1. This is due to higher interception deposition as the effective length (maximum projected length) increased with decreasing fractal dimension.

For fiber-like nanoparticles including nanofibers and multi-walled carbon nanotubes (MWCNT), interception deposition is higher than compact particles (Seto et al. 2010; Wang et al. 2011a,b; Son et al. 2014). Wang et al. (2011a) performed penetration measurement of single-fiber MWCNT classified by a differential mobility analyzer (DMA) in a model filter system consisting of 20 wire screens and numerical simulation of fiber penetration in the screen filter assuming random orientation of MWCNTs. Numerical results for MWCNTs agreed reasonably well with experimental data when the mobility diameter was less than 250 nm, but significantly underestimated the penetration when the mobility diameter was larger than 250 nm. The discrepancy was attributed to possible bending of the longer carbon nanotubes (CNTs) in the flow. They also performed similar experimental measurements of MWCNT single-fiber penetration through a screen filter and compared with a single-fiber filtration model (Wang et al. 2011b). They found out that the interception parameter using the random orientation of fiber underestimated the penetration for fiber longer than 100 nm. An effective interception length can be approximated by the MWCNT aerodynamic diameter by multiplying by a scaling factor.

There was limited information of physical characterizations and transport properties of nanoscale TiO_2 particles and how these characteristics influenced the particle transport and collection in filters. In a recent study, nanoscale TiO_2 particles were sampled using a MOUDI impactor (Noel et al. 2013). TEM analysis of collected samples on the MOUDI impactor stages showed compact agglomerates consisting of spherical primary particles. The projected area diameters on each impactor stage were determined. For nanoscale particles, additional characteristics such as mobility diameter and physical dimensions are needed to understand their behaviors. The main objective of this study was to perform detailed characterization of TiO_2 agglomerate particles including physical dimensions and transport properties generated from a dry powder aerosol generator and how these properties influence particle penetration in a screen filter.

Materials and methods

Aerosol generation and characterization

The anatase TiO_2 aerosol, with a purity >99% and 10–25 nm diameter (US Research Nanomaterials Inc., Houston, TX, USA), was used in the study. The TiO_2 aerosol

was generated by a dry powder dispersion method using a vortex shaker (Vortex Genie 2, Model G560, Scientific Industries Inc., Bohemia, NY, USA; Ku et al. 2006).

The aerosol was then classified by an Electrostatic Classifier (EC; Model 3071A, TSI Inc., Shoreview, MN, USA). Mobility diameters in the range of 50 to 500 nm were used for the characterization study. The classified CNT aerosol was verified by the Scanning Mobility Particle Sizer (SMPS; GRIMM Aerosol Technik GmbH & Co., Germany). Figure 1 shows the aerosol generation system.

The mobility classified TiO_2 particles were characterized in terms of effective density, mass, transport properties, and physical dimensions. A point-to-plane electrostatic precipitator (In-Tox Products, Moriarty, NM) was used to collect TiO_2 particles on TEM grids (Cheng et al. 1981). The acquired TEM grids loaded with TiO_2 aerosols were then analyzed by a transmission electron microscope (JEOL Model 2010, JEOL Ltd., Tokyo, Japan) at the University of New Mexico (UNM). Photomicrography taken by the TEM was then analyzed for physical dimensions and morphology using an imagine analysis software, Image-Pro Plus (v4.0, Media Cybernetics, Silver Spring, MD, USA).

Tandem mobility classification - mass analyzer measurement

An Aerosol Mass Analyzer (APM, Model 3601, Kanomax USA, Andover, NJ, USA) was used to measure the mobility-classified TiO_2 for its mass, effective density (ρ_{eff}), aerodynamic diameter, and dynamic shape factor following the method described by McMurry et al. (2002). Basically, polystyrene (PSL) particles were introduced into the APM and the concentration of PSL particles was measured downstream from the APM by varying the APM voltage. The APM voltage (V_{PSL}) corresponding to the peak concentration was the point where the centrifugal and electrostatic forces were in balance. Subsequently, classified TiO_2 aerosol of the same mobility was introduced to the APM and its peak concentration and voltage (V_{CNT}) was determined.

The effective density and mass of the TiO_2 particles are then calculated (McMurry et al. 2002; Park et al. 2003):

$$\rho_{eff} = \rho_{PSL} \frac{V_{CNT}}{V_{PSL}} \quad [1]$$

$$m = \frac{\pi \rho_{eff} d_M^3}{6} \quad [2]$$

The aerodynamic diameter of the classified TiO_2 was estimated as follows (Kasper 1982; Park et al. 2003):

$$d_{ae} = d_M \sqrt{\frac{\rho_{eff}\, C(d_M)}{\rho_o\, C(d_{ae})}}, \quad [3]$$

where d_{ae} and d_M are the aerodynamic and mobility diameter of the classified TiO_2; $C(d_{ae})$ and $C(d_M)$ are the

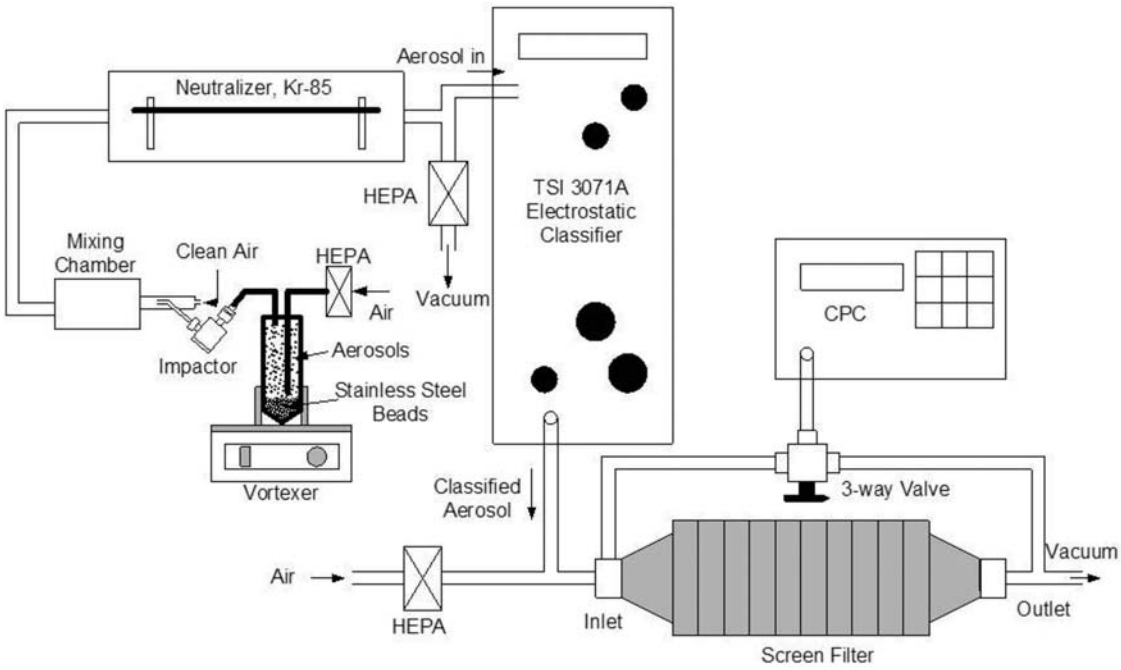

Figure 1. The schematic diagram of the experimental setup with the screen filter.

corresponding slip correction factors for d_{ae} and d_M, respectively; and ρ_o is the unit density.

Penetration of TiO_2 in a screen filter

A screen filter consisting of 30 stainless mesh 635 wire screens (Tetko Inc., Monterey Park, CA, USA) was used for the filtration study. These wire screens were used in filtration studies of MWCNT (Wang et al. 2011a,b) and utilized in the diffusion battery (Model 3040, TSI Inc.). The screen was characterized extensively in terms of fiber diameter (20 μm), thickness (50 μm), and solid volume fraction (0.345) (Cheng and Yeh 1980; Cheng et al. 1980; Wang et al. 2011a). Penetration of mobility-classified TiO_2 particles through the screen filter was measured with a condensation particle counter (GRIMM Technologies, Inc., Douglasville, GA, USA). The flow rates through the filter were 2 and 4 L/min, corresponding to face velocities of 2.92 and 5.85 cm/s, respectively.

Fan model filtration theory

The screen filter has been shown in physical structure to be a good example of fan model filter (FMF), which consists of parallel rows of monodisperse cylinders placed perpendicular to the air flow (Cheng and Yeh 1980). In the same plane, the cylinders are parallel and equidistant, but axes of cylinders in different planes are oriented randomly. Also, the pressure drop and filtration efficiency for spherical particles of screen filters follows the FMF (Cheng and Yeh 1980; Cheng et al. 1980, 1985). Cheng et al. (1985) reported that the measured pressure drop of screen filters follows the FMF (Kirsch and Fuchs 1967):

$$\Delta P = F\left(\frac{4U\mu\alpha H}{\pi d_W^2}\right) = \frac{4\pi}{K_F}\left(\frac{4U\mu\alpha H}{\pi d_W^2}\right), \quad [4]$$

where F is the dimensionless drag, U is the face velocity in filter, μ is the air viscosity, α the solid volume fraction, d_W is the screen wire diameter, and H is the screen filter thickness. The Kuwabara hydrodynamic factor, K_F for the FMF is defined as

$$\begin{aligned} K_F &= -\frac{\ln \alpha_F}{2} - 0.75 + \alpha_F - \frac{\alpha_F^2}{4} \\ &= -0.5 \ln \alpha - 0.52 + 0.64\,\alpha. \end{aligned} \quad [5]$$

In the FMF, α is replaced by α_F (= α π/2) in Equation (5), indicating a lower pressure drop than a filter consisting of parallel staggered rows (Kirsch and Fuchs 1967).

Based on mass conservation, the classical single-fiber filtration theory is expressed as

$$P = \frac{C_{out}}{C_o} = \exp\left[-\frac{4 \propto nH}{\pi(1-\alpha)d_W} E_{\text{single fiber}}\right], \quad [6]$$

where C_o and C_{out} are the initial concentration and concentration exiting from the filter, respectively, and n is the number of screens. The single-fiber efficiency is the summation of individual efficiencies for diffusion (E_D), direct interception (E_R), initial impaction (E_I), and an interaction term for diffusion and interception (E_{DR}) (Stechkina et al. 1969):

$$E_{\text{single fiber}} = E_D + E_R + E_I + E_{DR}. \quad [7]$$

For FMF, the individual term in Equation (7) can be expressed as (Stechkina et al. 1969; Cheng et al. 1980; Kirsch and Chechuev 1985):

$$E_D = 2.7\, Pe^{-2/3}, \quad [8]$$

$$E_R = \frac{1}{2K_F}\left[\left(\frac{1}{1+R}\right) - (1+R) + 2(1+R)\ln(1+R)\right], \quad [9]$$

$$E_I = \frac{1}{4K_F^2}\left[(29.6 - 28\alpha^{0.62})R^2 - 27.5R^{2.8}\right]\text{Stk}, \quad [10]$$

$$E_{DR} = 1.24\,(K_F)^{-1/2} Pe^{-1/2} R^{2/3}. \quad [11]$$

The Peclet number (Pe), the interception parameter (R), and the Stokes number (Stk) are defined as

$$Pe = \frac{Ud_W}{D} \quad [12]$$

$$R = \frac{d_p}{d_w}, \quad [13]$$

$$\text{Stk} = \frac{\rho_o d_{ae}^2\, C(d_{ae})U}{18\mu d_w}, \quad [14]$$

where D is the diffusion coefficient of the particle, C is the slip correction factor, d_p is the particle physical diameter, ρ_o is unit density, and d_{ae} is the aerodynamic diameter.

Experimental filtration efficiencies in several screen filters showed that the FMF single-fiber filtration equation is valid for spherical particles in the size range of 2 to 900 nm (Cheng et al. 1980, 1985; Kirsch and Chechuev 1985; Ichitsubo et al. 1996).

Results and discussion

Morphology and physical dimension measurement

Figure 2 shows examples of mobility-classified TiO_2 particles collected on TEM grids. Compact agglomerates consisting of primary particles were observed for mobility diameters between 50 and 500 nm, similar to those reported in the plants handling nanoscale TiO_2 materials (Curwin and Bertke 2011; Koivisto et al. 2012). Also, several inhalation studies of rodents exposed to nanoscale TiO_2 particles showed that laboratory-generated particles have compact agglomerates in the 100 to 500 nm size range using either a Collison nebulizer (Grassian et al. 2007) or dry powder generators including a brush dust generator (Ma-Hock et al. 2009), a fluidized bed, and rotating brush generator (RBG; Noel et al. 2013). These studies did not report measurements of TiO_2 physical dimensions. Detailed measurements of physical dimensions of the classified TiO_2 nanoparticles and their relationship to the mobility diameter were described in the following section.

The measured physical dimensions included the maximum length (L), maximum projected width (W) normal to L, Aspect ratio (L/W), and the projected diameter calculated from the projected area. The length is also called the maximum Feret diameter and W is the Feret diameter normal to the maximum Feret diameter. Table 1 lists the mean and standard deviation of the measured dimensions as a function of mobility diameter. Figure 3 plots mean length and projected area diameter (d_{pa}) as function of mobility diameter (d_M), showing that both length and diameter increased with the mobility diameter. The relationship of d_{pa} and mobility diameter can be expressed as a linear equation:

$$d_{pa} = 8.22 + 0.998 d_M. \quad [15]$$

The coefficient of determination, R^2 was 0.934. The projected area diameter is similar but slightly larger than the mobility diameter, consisting with the theoretical model and experimental observations (Rogak and Flagan 1993; Kim and Zachariah 2005; Kim e al. 2007). Figure 4 plots the mean aspect ratio as a function of d_M. The mean aspect ratio was relatively constant between 1.39 and 1.55 in the size range of 50 to 400 nm, indicating that these are compact agglomerates. The mean and standard deviation of the aspect ratio (β) was 1.50 and 0.06, respectively.

Table 1. Physical dimensions of TiO_2 nanoparticles.

Mobility diameter (nm)	L (nm)	SD	d_{pa} (nm)	SD	Aspect ratio	SD
56.7	129	50.7	93.7	19.2	1.51	0.30
111	161	48.2	122	34.7	1.48	0.32
152	171	71.1	125	46.4	1.55	0.44
231	322	73.8	244	74.8	1.51	0.35
308	365	139	274	134	1.54	0.35
380	528	192	426	148	1.39	0.30

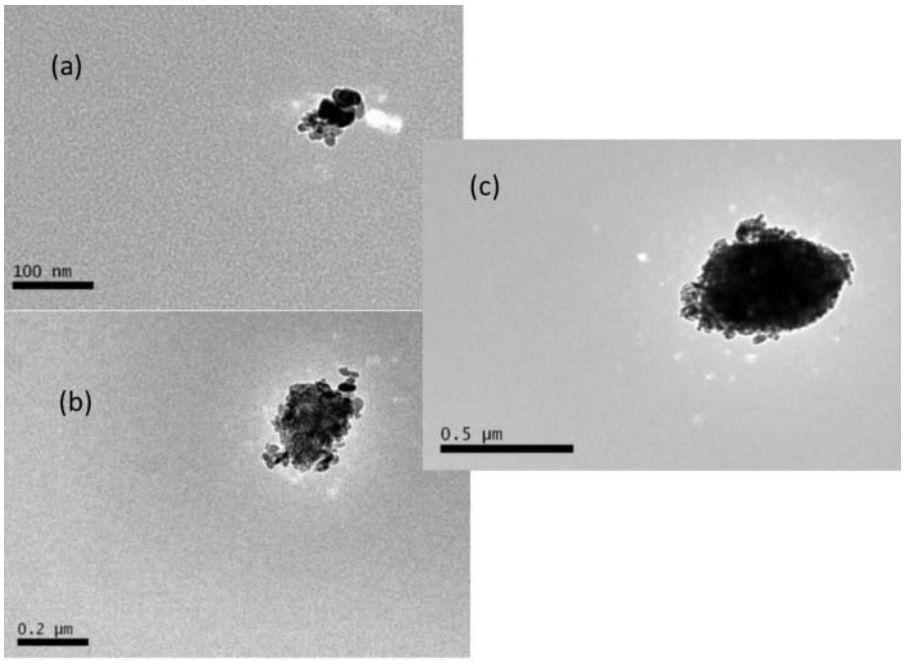

Figure 2. Examples of the TEM morphology of the TiO_2 particle for mobility diameter of 50 nm (a), 200 nm (b), and 500 nm (c).

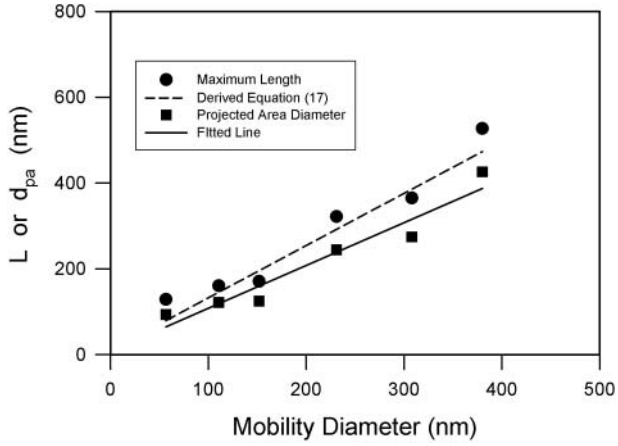

Figure 3. Physical dimension measured from the TEM images including the maximum length (L) and the projected area diameter (d_{pa}) of TiO_2 nanoparticles.

Assuming an elliptical shape with constant aspect ratio for the projected area of TiO_2 nanoparticles, d_{pa} can be expressed as

$$d_{pa} = \sqrt{\frac{L^2}{\beta}}. \quad [16]$$

By substituting Equation (15) into Equation (16) and using the mean value of β, we obtain the following equation:

$$L = 10.1 + 1.22 d_M. \quad [17]$$

Figure 3 shows that Equation (17) is in agreement with the experimental data with R^2 of 0.906. Chen et al. (2015) also reported linear relationship between the maximum length and mobility diameter for silver aggregate nanoparticles of various shapes.

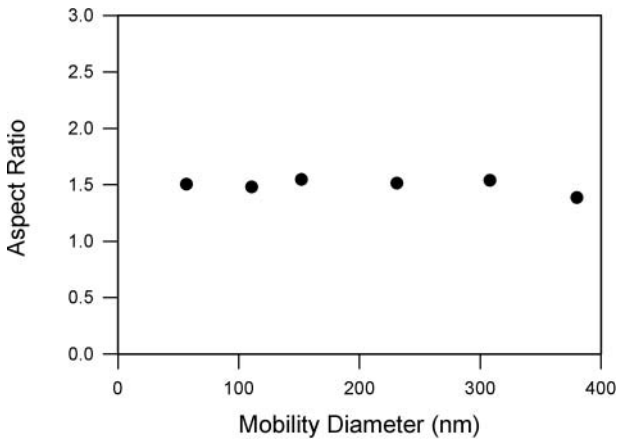

Figure 4. Aspect ratio plotted as a function of mobility diameter.

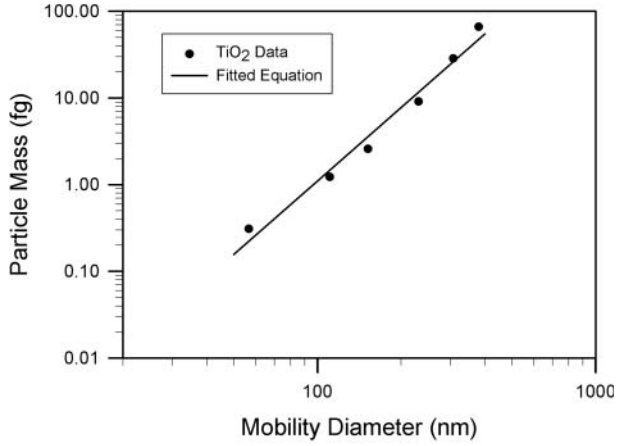

Figure 5. The TiO_2 particle mass as a function of mobility diameter. The solid line is the fitted power (Equation (17)).

APM measurement

From the APM measurement of the mobility classified TiO_2 particle, the aerodynamic diameter was then estimated using Equation (3). The particle mass was plotted as a function of the mobility diameter in a log–log scale as shown in Figure 5. The mass–mobility diameter followed a power-law relationship:

$$m = a d_M^{D_f}. \quad [18]$$

The slope of the fitted equation (D_f) is the fractal dimension based on mass–mobility diameter and had a value of 2.82. The R^2 value of the fitted equation was 0.974. The value of the D_f is close to 3 for spherical particle, consistent with the compact shape obtained from the TEM photos.

Penetration through the filter

Figure 6 shows the penetration of TiO_2 particles through the screen filter as a function of mobility diameter. Three measurements were conducted for each experimental condition. Penetration increased with mobility diameter and seemed to level off at larger diameters. Penetrations for 5.85 cm/s were higher than those obtained at 2.92 cm/s, indicating the diffusion and interception were the main filtration mechanisms. To further investigate the relationship between the particle characteristics and the penetration through the screen filter, the fan model filtration theory for screen filters was adopted for the TiO_2 particles. Also shown in Figure 6 is penetration of spherical particles at 5.85 cm/s reported by us previously (Cheng et al. 1985). Penetration of TiO_2 particles follows closely with the spherical data for small particles up to

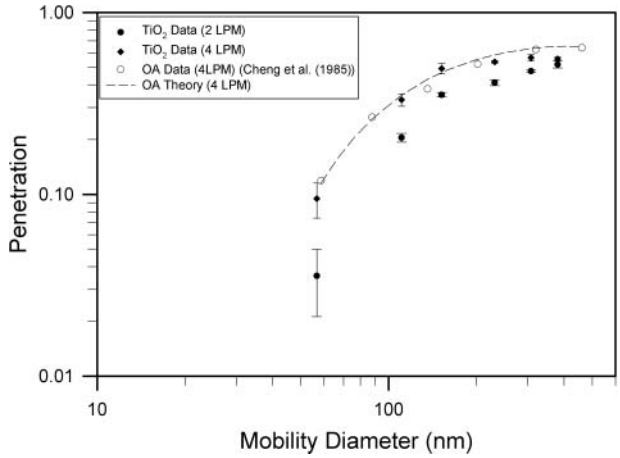

Figure 6. Experimental penetration of TiO_2 aerosol (mean ±SD) in the screen filter as a function of mobility diameter at face velocities of 2.92 and 5.85 cm/s, respectively. Also shown is the penetration data of oleic acid (OA) spherical particle at 5.85 cm/s as well as the theoretical calculation.

200 nm. For particles larger than 200 nm, the TiO_2 penetration is slightly lower than those of spherical particles.

Penetration based on the single-fiber filtration model (Equations (6)–(14)) for the screen filter used in this study ($\alpha = 0.345$, $d_w = 20$ μm, and $H = 50$ μm) is shown in Figure 6 for spherical particles at 5.85 cm/s, indicating that the FMF theory agrees with the experimental data. Figure 7 shows penetration curves for TiO_2 particles based on the single-fiber filtration models. All parameters for TiO_2 particles were based on measurements. The diffusion coefficient was based on the mobility diameter; the aerodynamic diameter was given in

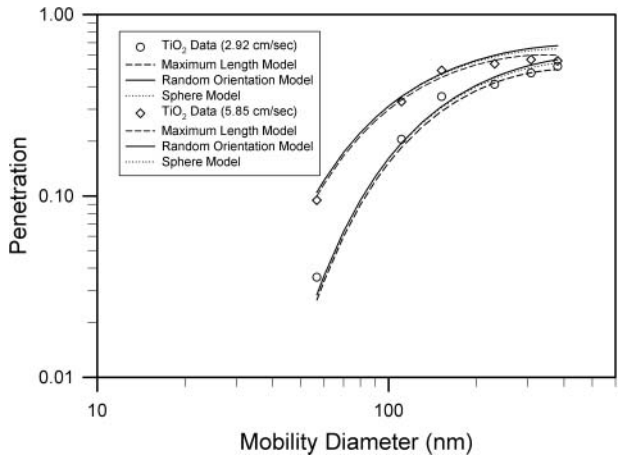

Figure 7. The curves are single fiber theoretical filtration models using different dimensions for the interception parameter. The mobility diameter was used in the interception parameter in Model 1 (dotted curve). In Model 2 (solid curve), random orientation of the particle was assumed. In Model 3 (dashed curve), the L was used in the interception parameter.

Equation (3). For the interception parameter (Equation (13)), three different scales of d_p were used, including: (1) $d_p = d_M$ assuming a spherical particle shape, (2) $d_p = L \sin\theta \cong 0.63$ L assuming random orientation of the TiO_2 particle, and $d_p = L$ (maximum length). Figure 7 shows that penetrations calculated from all three models based on different interception parameters were close because TiO_2 were compact nanoparticles of small aspect ratio. The penetrations diverged only for diameter >200 nm when the interception mechanism became more important in the filtration of TiO_2 nanoparticles. Experimental penetration data of TiO_2 particles agreed with calculations from all three models for particle size smaller than 150 nm. For particle sizes >200 nm, the experimental data were in best agreement with the model in which the maximum length was used to calculate the interception model.

TiO_2 nanoparticles used in this study had a mass–mobility fractal dimension of 2.82 close to the spherical shape ($D_f = 3.0$). TiO_2 penetrations in the screen filter were slightly lower than spherical particles. This result was consistent with the data on penetration of silver nanoparticles in a Nuclepore filter (Chen et al. 2015). Their data showed that penetrations decreased as the mass–mobility fractal dimension decreased from 3.0 to 2.1; penetration of aggregates with $D_f = 2.6$ was close to that of silver particles of spherical shape ($D_f = 3.0$). When the maximum length was used in the interception parameter, our single fiber model was in agreement with TiO_2 experimental data. These results were consistent with previous filtration studies for silver chain agglomerates (Kim et al. 2009), who reported that the penetration data agreed with a filtration model, where the interception parameter was calculated based on the maximum length. Wang et al. (2011b) indicated that using the maximum geometric length to calculate the interception parameter would be reasonable when the rotation time of a non-spherical particle was much less than the transport time for the particle to pass through the filter fiber. The silver chain agglomerates had an aspect ratio of 1.6–1.8 (Kim et al. 2009), where the TiO_2 nanoparticles in this study had an aspect ratio of 1.39–1.55. Both nanoparticles had small aspect ratios and hence, short rotational time (Wang et al. 2011b). More recently, in a capillary tube model of penetration for MWCNT through a Nuclepore filter, the maximum length of MWCNT was used in the interception parameter, which agreed with experimental data (Chen et al. 2014). The capillary tube was relatively long (11 μm) compared with MWCNT (30–500 nm diameter); therefore MWCNT might have enough time to rotate during the time flying through the tube. This might also be valid in the case of screen filter diameter (20 μm) and TiO_2 (50–400 nm).

Conclusions

Detailed characterization of TiO_2 particles generated from a dry powder generator was performed. Analysis of TEM photos of mobility-classified TiO_2 particles showed compact agglomerates of nanoscale primary particles. The physical shape obtained in this study is similar to TiO_2 particles observed in production facilities (Curwin and Bertke 2011; Koivisto et al. 2012) as well as TiO_2 generated in the laboratory for inhalation exposure studies (Grassian et al. 2007; Ma-Hock et al. 2009; Noel et al. 2013). The projected area diameter is close to the mobility diameter, where the length is about 30% larger than the mobility diameter. The mean aspect ratio of the TiO_2 agglomerate was constant and small between 1.39 and 1.55. Using the tandem DMA-APM technique, we were able to measure aerodynamic diameter, mass, and the fractal dimension. The value of fractal dimension based on mass–mobility diameter was 2.82, consistent with the observed compact shape.

Penetration of classified TiO_2 particles through a screen filter was measured. Penetration increased with increasing mobility diameter and flow rate indicating that diffusion and interception were the main filtration mechanisms. The measured physical dimensions, mobility diameter, and aerodynamic diameter were used in a single-fiber filtration theory for the fan model filter to predict the penetration of TiO_2 particles. The mobility diameter, maximum length (L), and 0.63 L assuming radon orientation were used in the interception parameter. Penetrations calculated from all three models based on these interception parameters were close because TiO_2 were compact nanoparticles of a small aspect ratio. Experimental penetration data of TiO_2 particles agreed with calculations from all three models for particle size smaller than 150 nm. For particle sizes >200 nm, the experimental data were in best agreement with the model in which the maximum length was used to calculate the interception model. This result was consistent with previous filtration study for silver nanoparticle chain agglomerates of aspect ratio of 1.6–1.8 (Kim et al. 2009). It may be because the rotation time of a non-spherical particle of a small aspect ratio was much less than the transport time for the particle to pass through the filter fiber.

Funding

This research was sponsored by U.S. NIOSH grant R01 OH009801 and R01 OH010062.

References

Boffetta, P., Soutar, A., Cherrie, J. W., Granathe, F., Andersen, A., Anttila, A., Blettner, M., Gaborieau, V., Klug, S. J., Langard, S., Luce, D., Merletti, F., Miller, B., Mirabelli, D., Pukkala, E., Adami, H. O., and Weiderpass, E. (2004). Mortality Among Workers Employed in the Titanium Dioxide Production Industry in Europe. *Cancer Causes Control*, 15:697–706.

Chen, S. C., Wang, J., Bahk, Y. K., Fissan, H., and Pui, D. Y. H. (2014). Carbon Nanotube Penetration Through Fiberglass and Electret Respirator Filter and Nuclepore Filter Media: Experiments and Models. *Aerosol Sci. Technol.*, 48:997–1008.

Chen, S. C., Wang, J., Fissan, H., and Pui, D. Y. H. (2015). Optimizing Filtration Experiments for Length and Fractal Dimension Characterization of Non-Spherical Particles. *Aerosol Sci. Technol.*, 49:547–555.

Cheng, Y. S., Keating, J. A., and Kanapilly, G. M. (1980). Theory and Calibration of a Screen-Type Diffusion Battery. *J. Aerosol Sci.*, 11:549–556.

Cheng, Y. S., and Yeh, H. C. (1980). Theory of a Screen-Type Diffusion Battery. *J. Aerosol Sci.*, 11:313–320.

Cheng, Y. S., Yeh, H. C., and Brinsko, K. J. (1985). Use of Wire Screens as a Fan Model Filter. *Aerosol Sci. Technol.*, 4:165–174.

Cheng, Y. S., Yeh, H. C., and Kanapilly, G. M. (1981). Collection Efficiencies of a Point-to-Plane Electrostatic Precipitator. *Am. Ind. Hyg. Assoc. J.*, 42:605–610.

Curwin, B., and Bertke, S. (2011). Exposure Characterization of Metal Oxide Nanoparticles in the Workplace. *J. Occup. Environ. Hyg.*, 8:580–587.

Fryzek, J. P., Chadda, B., Marano, D., White, K., Schweitzer, S., McLaughlin, J. K., and Bolt, W. J. (2003). A Cohort Mortality Study Among Titanium Dioxide Manufacturing Workers in the United States. *J. Occup. Environ. Med.*, 45:400–409.

Grassian, V. H., O'Shaughnessy, P. T., Adamcakova-Dodd, A., Pettibone, J. M., and Thorne, P. S. (2007). Inhalation Exposure Study of Titanium Dioxide Nanoparticles with a Primary Particle Sizes of 2 to 5 nm. *Environ. Health Perspect.*, 115:397–402.

Heinrich, U., Fuhst, R., Rittinghausen, S., Creutsenberg, O., Bellmann, B., Koch, W., and Levsen, K. (1995). Chronic Inhalation Exposure of Wistar Rats and Two Different Strains of Mice to Diesel Engine Exhaust, Carbon Black, and Titanium Dioxide. *Inhal. Toxicol.*, 7:533–556.

Huang, C. H., Tai, C. Y., Huang, C. Y., Tsai, C. J., Chen, C. W., Chang, C. P., and Shih, T. S. (2010). Measurements of Respirable Dust and Nanoparticle Concentrations in a Titanium Dioxide Pigment Production Factory. *J. Environ. Sci. Health Part A*, 45:1227–1233.

Ichihara, S., Li, W., Omura, S., Fujitani, Y., Liu, Y., Hiraku, Y., Hisanaga, N., Wakai, K., Ding, X., Kobayashi, T., and Ichihara, G. (2016). Exposure Assessment and Heart Rate Variability Monitoring in Workers Handling Titanium Dioxide Particles: A Pilot Study. *J. Nanopart. Res.*, 18:52–66.

Ichitsubo, H., Hashimoto, T., Alonso, M., and Kousaka, Y. (1996). Penetration of Ultrafine Particles and Ion Clusters Through Wire Screen. *Aerosol Sci. Technol.*, 24:119–127.

Kasper, G. (1982). Dynamics and Measurement of Smokes: II. The Aerodynamic Diameter of Chain Aggregates in the Transition Regime. *Aerosol Sci. Technol.*, 1:201–215.

Kim, S. C., Harrington, M. S., and Pui, D. Y. H. (2007). Experimental Study of Nanoparticles Penetration Through Commercial Filter Media. *J. Nanopart. Res.*, 9:117–125.

Kim, S. C., Wang, J., Emery, M. S., Shin, W. G., Mulholland, G. W., and Pui, D. Y. H. (2009). Structural Property Effect of

Nanoparticle Agglomerates on Particle Penetration Through Fibrous Filter. *Aerosol Sci. Technol.*, 43:344–355.

Kim, S. H., and Zachariah, M. R. (2005). In-flight Size Classification of Carbon Nanotubes by Gas Phase Electrophoresis. *Nanotechnology*, 16:2149–2152.

Kirsch, A. A., and Chechuev, P. V. (1985). Diffusion Deposition of Aerosol in Fibrous Filters at Intermediate Peclet Numbers. *Aerosol Sci. Technol.*, 4:11–16.

Kirsch, A. A., and Fuchs, N. A. (1967). Studies on Fibrous Aerosol Filters - II. Pressure Drops in Systems of Parallel Cylinders. *Ann. Occup. Hyg.*, 10:23–30.

Koivisto, A. J., Lyyranen, J., Auvinen, A., Vanhala, E., Hameri, K., Tuomi, T., and Jokiniemi, J. (2012). Industrial Worker Exposure to Airborne Particles During the Packing of Pigment and Nanoscale Titanium Dioxide. *Inhal. Toxicol.*, 24:839–849.

Ku, B. K., Emery, M. S., Maynard, A. D., Stolzenburg, M. R., and McMurry, P. H. (2006). In Situ Structure Characterization of Airborne Carbon Nanofibres by a Tandem Mobility-Mass Analysis. *Nanotechnology*, 17:3613–3621.

Lee, J. H., Kwon, M., Ji, J. H., Kang, C. S., Ahn, K. H., Han, J. H., and Yu, I. J. (2011). Exposure Assessment of Workplaces Manufacturing Nanosized TiO2 and Silver. *Inhal. Toxicol.*, 23:226–236.

Lee, K. P., Trochimowicz, H. J., and Reinhardt, C. F. (1985). Pulmonary Response of Rats Exposed to Titanium Dioxide (TiO2) by Inhalation for Two Years. *Toxicol. Appl. Pharmacol.*, 79:179–192.

Ma-Hock, L., Burkhardt, S., Strauss, V., Gamer, A. O., Wiench, K., van Ravenzwaay, B., and Landsiedel, R. (2009). Development of a Short-Term Inhalation Test in the Rat Using Nano-Titanium Oxide as a Model Substance. *Inhal. Toxicol.*, 21:102–118.

McMurry, P. H., Wang, X., Park, K., and Ehara, K. (2002). The Relationship Between Mass and Mobility for Atmospheric Particles: A New Technique for Measuring Particle Density. *Aerosol Sci. Technol.*, 36:227–238.

NIOSH. (2011). *Occupational Exposure to Titanium Oxide. Anonymous National Institute for Occupational Safety and Health*, CDC, Cincinnati, OH.

Noel, A., L'Esperance, G., Cloutier, Y., Plamondon, P., Boucher, J., Philippe, S., Dion, C., Truchon, G., and Zayed, J. (2013). Assessment of the Contribution of Electron Microscopy to Nanoparticle Characterization Sampled with Two Cascade Impactors. *J. Occup. Environ. Hyg.*, 10:155–172.

Park, K., Cao, F., Kittelson, D. B., and McMurry, P. H. (2003). Relationship between Particle Mass and Mobility for Diesel Exhaust Particles. *Environ. Sci. Technol.*, 37:577–583.

Rengasamy, A., Eimer, B., and Shaffer, R. E. (2009). Comparison of Nanoparticle Performance of NIOSH-Approved and CE Marked Filtering-Facepiece Respirators Against 4–30 Nanometer Size Nanoparticles. *Ann. Occup. Hyg.*, 53:117–128.

Robichaud, C. O., Uyar, A. E., Darby, M. R., Zucker, L. G., and Wiesner, M. R. (2015). Estimates of Upper Bounds and Trends in Nano-TiO2 Production as a Basis for Exposure Assessment. *Environ. Sci. Technol.*, 15:4227–4233.

Rogak, S. N., and Flagan, R. C. (1993). The Mobility and Structure of Aerosol Agglomerates. *Aerosol Sci. Technol.*, 18:25–47.

Seto, T., Furukawa, T., Otani, Y., Uchida, K., and Endo, S. (2010). Filtration of Multi-Walled Carbon Nanotube Aerosol by Fibrous Filters. *Aerosol Sci. Technol.*, 44:734–740.

Son, M., Park, H., Park, M., Wang, J., and Shin, W. G. (2014). Silver Nanowire Penetration Through Screen Filter. *Aerosol Sci. Technol.*, 48:480–488.

Stechkina, I. B., Kirsch, A. A., and Fuchs, N. A. (1969). Investigations of Fibrous Filters for Aerosol Filters–IV Calculation of Aerosol Deposition in Model Filters in the Region of Maximum Particle Breakthrough. *Ann. Occup. Hyg.*, 12:1–8.

Wang, J., Kim, S. C., and Pui, D. Y. H. (2011a). Carbon Nanotube Penetration Through a Screen Filter: Numerical Modeling and Comparison with Experiments. *Aerosol Sci. Technol.*, 45:443–452.

Wang, J., Kim, S. C., and Pui, D. Y. H. (2011b). Measurement of Multi-Wall Carbon Nanotube Penetration Through a Screen Filter and Single-Fiber Analysis. *J. Nanopart. Res.*, 13:4565–4573.

Zhou, Y., and Cheng, Y. S. (2016). Evaluation of N95 Filtering Facepiece Respirators Challenged with Engineered Nanoparticles. *Aerosol Air Qual. Res.*, 16:212–220.